J Math Model Algor (2014) 13:355–369
DOI 10.1007/s10852-014-9252-1

Image-Filtering and Optimization of Rainy Cells

O. Raaf · A. Adane

Received: 10 August 2013 / Accepted: 6 February 2014 / Published online: 10 June 2014
© Springer Science+Business Media Dordrecht 2014

Abstract This paper deals with the identification and elimination of ground echoes in radar images using their textural features. The images collected in Setif (Algeria) by a non Doppler radar, are processed. Two kinds of texture-based techniques have been considered, consisting in calculating either the histograms of their sum and difference or the pattern recognition. Energy and local homogeneity are found to be the textural parameters that clearly separate the precipitation and ground echoes. To get only the rainfall echoes, the resulting template is applied to each of the raw radar images and the filtering is improved by removing the residual clutter with pattern recognition. This method allows as to completely removing the ground clutter with minimal alterations of the rain echoes with reduced calculation time. It has the advantages of effectiveness and simplicity. However, when there is overlap of precipitation echoes with the ground echoes, significant small cells may occur. In this case, these cells are restored by interpolating from neighboring pixels with a regularization function. The application of this optimization algorithm of filtered images can effectively reproduce true structure of clouds. The radar images can be processed in real-time because the computation time needed by these techniques is small.

Keywords Ground echoes · Optimization · Pattern recognition · Radar images · Textural features · Template

1 Introduction

The climatic changes observed from the beginning of the third millennium till to-day, have made necessary the weather forecast in real time. In these conditions, rainfall previsions are mostly deduced from visual cloud observations and rainfall measurements insured by the

O. Raaf (✉) · A. Adane
Faculty of Electronics and Computer, Laboratory of Image Processing and Radiation,
University of Science and Technology H. Boumediene (USTHB),
P.O. Box 32, El-Alia, 16111, Algiers, Algeria
e-mail: oraaf@usthb.dz; rf_ouarda@yahoo.fr

meteorological network equipped with automatic measurement systems and remote sensing tools [1, 2]. But, the accuracy of such previsions obviously depends on the number of rainfall gauges used and their repartition over the country. In particular, different geostationary satellites intended to meteorological observations, orbit the Earth in the equatorial plane for about thirty years. Thanks to the satellite and radar observations, better previsions can be performed in space and time. The images collected by meteorological satellites and radars are often infected by noise due to the environment, the data acquisition devices and the transmission system used. These images carry information about weather, which must be cleared up. In general, the filtering techniques applied to scrambled images aim at giving them a better visual aspect. The filtering of images taken by weather radar consists in distinguishing between the rainfall echoes and those coming from the ground. Indeed, the useful signal received at the input of weather radar is that which characterizes the images of precipitation. Most meteorological radars designed for the detection of precipitation fields, work by producing pulse sine waves in the microwave band, are non-coherent and scan the environment with a radius of several ten kilometers. Numerical images yielding the position, size, shape and intensity of precipitation and ground echoes, are usually collected every five minutes (or more) by these radars in the horizontal plane. This kind of radar images is very useful to evaluate the precipitation fields, follow their evolution and in particular, prevent severe atmospheric phenomena such as hailstorms and tornados. Thus, in the presence of obstacles, in particular, close to mountainous areas, the use of this radar appears difficult because of the presence of terrestrial relief which amends and sometimes prevents the propagation of radar waves.

The influence of the Relief is very detrimental to the measurement of rainfall with radar. Ground clutter is visible on all images regardless of the location of the radar during all season of acquisition. It is therefore essential to make adequate filtering to remove these echoes coming from the ground. Several Technical have been proposed in the literature to eliminate the ground clutter [3–8]. These removal processes are based on the Doppler filtering, the logarithmic amplification, the comb filter, the attenuation of the signal, thresholding, spectral technique or the natural properties of these echoes that is their texture, shape, evolution over the time and the distance from the radar.

In particular, texture analysis is known to be among the most efficient statistical approaches [9–15]. To account for the texture of an image, this analysis mainly consists in evaluating the joint probability $P(i, j/d, \theta)$ that two pixels having respective grey levels i and j, are distant of length d from one to the other, following an orientation angle θ with respect to the horizontal direction. A grey level co-occurrence matrix (GLCM) is therefore built with elements which are the joint probabilities obtained for all the possible pairs of pixels at given distance d and angle θ. Such a matrix is used to evaluate statistical parameters such as the fourteen initially defined by Haralick in 1979 to characterize the image texture [10]. In practice, the textural parameters are evaluated for 8-neighborhood, after averaging the co-occurrence matrices previously computed for $d = 1$ and $\theta = 0°, 45°, 90°$ and $135°$. The GLCM-based method is very efficient but implies tedious calculations essentially due to the double summation and therefore, needs an important computation memory. Fortunately, there are methods like GLDV (Grey Level Difference vector) and SADH (Sum And Difference Histograms) which are also based on the calculation of the joint probabilities of pairs of pixels, but require only the computation of only simple sums [11, 12]. Consequently, both methods have the advantage of reducing the memory size and the computation time strongly. To identify the types of radar echo, we have then chosen to implement the SADH approach. The GLDV technique derived by Wezka et al. (1976) amounts to calculate the histogram of the absolute difference between the grey levels of pairs of pixels [11].

The SADH approach is due to Unser [12] who applied a suitable orthogonal transformation consisting in replacing the joint probabilities $P(i, j/d, \theta)$ by the sum and difference histograms of grey levels i and (j) [12]. In Algeria, Ameur et al. [15] have successfully used this method to segment Meteosat images and identify the soils, seas and clouds appearing in these images [15]. In our laboratory, Haddad et al. (2004) have filtered rainfall and ground echoes collected by three different meteorological radar using GLDV and SADH [9]. In general, GLCM and SADH are found to yield comparable results whereas GLDV operates faster, but is slightly less accurate. As we have already digital radar images and considering the difference of the physical properties between rain and ground echoes, the methods we have chosen to filter our radar images are texture analysis, and an original method based on templates associated with pattern recognition. Under these conditions, we first briefly describe the principle of the SADH. After that we develop our new method based on the template associated with the pattern recognition and then we present the results obtained after applying the filter. In a second part, we present the method that allowed us to remove the gaps left after filtering interpolating from the neighboring pixels thanks to a regularization function of split Bregman.

2 Data Base

Since 1996, the images under study were collected every 15 min by an ASWR 81 radar (Algerian Service Weather Radar) installed at the top of Meghres mountain, near the town of Setif (the capital of the High Tablelands lying at the north east of Algeria). This radar works at 5.6 GHz. Every 4 ms, it produces 250 peak-kW pulses during 4 μs. Its geographical coordinates are 36°11'N of latitude, 5°25E of longitude and 1730 m of altitude. The obtained images are recorded following the PPI (Plan Position Indicator) mode. Each of them consists of 512 × 512 pixels and the reflectivity of each pixel is encoded following sixteen color levels. For better clarity of viewing images, the black background has been replaced by the color white. Referring to the Lambert cards we added the outline of the coast. Then we calibrated these images in terms of latitude and longitude. Figure 1 shows an example of raw images taken in Setif during a bad weather conditions. This image shows especially the importance of ground clutter observed in the region of Setif and describing the mountainous terrain of the region. Indeed, Western Setif an orange band chain representing Djurdjura whose highest point is Mount Lalla Khadija (2308 m) is observed. South and North of the radar, bluish areas are observed corresponding to chains of Bibans and Babors respectively.

3 Filtering by Texture Analysis: the SADH Method

3.1 Methodology

Let the pixels i and j be at the coordinates (m, n) and (m', n') respectively and consider the random variables $y_{m,n}$ and $y_{m',n'}$ describing their respective histograms. Let us recall that m, n, m' or $n' = 1, \ldots, 512$, with $m' = m + dcos\theta$ and $n' = n + dsin\theta$ and i or $j = 0, 1, \ldots, 15$ for the images under study. The probability that the pairs of grey levels i and j are separated by distance d, following the orientation θ is:

$$P\,(i, j/d, \theta) = P\left(y_{m,n} = i, y_{m+d\cos\theta, n+d\sin\theta} = j\right) \quad (1)$$

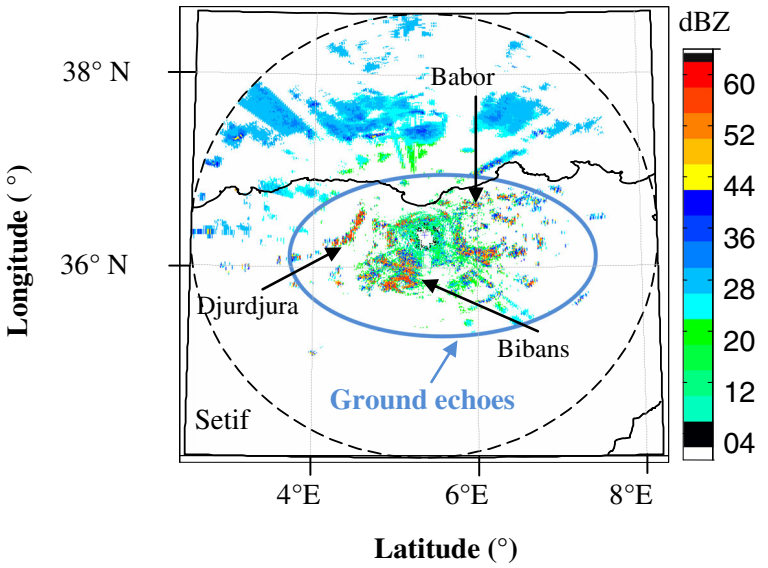

Fig. 1 Radar images collected in Setif in the rainy period

The co-occurrence matrix used to process the textural features of these images is then deduced from all the joint probabilities given by Eq. (1). Two new random variables, namely the sum and difference of grey levels, can be written as: [10, 12]

$$s_{m,n} = y_{m,n} + y_{m+\Delta x,n+\Delta y} \tag{2}$$

$$d_{m,n} = y_{m,n} - y_{m+\Delta x,n+\Delta y} \tag{3}$$

Probability distribution functions $P_s(i)$ and $P_d(j)$ then describe the resulting histograms of the sum and difference of grey levels respectively. Taking into account their symmetry properties, eight co-occurrence matrices are obtained for $\theta = 0°, 45°, 90°, 135°$. Fourteen statistical parameters usually give information about the image texture. However, mean, variance, energy, contrast, correlation, entropy, local homogeneity and kurtosis are the more commonly employed. Indeed, thanks to the display of an image sequence by the animation software, we found that the ground echoes are fixed, intense and localized while the rain echoes are mobile, occupy large areas with lower reflectivity and change shape. When processing the radar images, taken in Setif region, the energy W and local homogeneity Γ are found to be the best way for filtering the radar echoes. Let us recall that these textural parameters are, by definition, expressed as [12]:

$$W = \sum_i P_s(i)^2 \sum_j P_d(j)^2 \tag{4}$$

$$\Gamma = \sum_j \frac{1}{1+j^2}.P_d(j) \tag{5}$$

4 Identification and Filtering the Radar Echoes

The decision rule chosen to identify the types of radar echo is different from that based on the calculation of a similarity distance, as commonly used in automatic image classification. Briefly, it firstly consists in splitting the database recorded at Setif, into two subsets of radar images where appear either rainy clouds or none of them respectively (See Fig. 2). This preliminary classification facilitates the identification of the ground and rainfall echoes. The textural parameters given by Eqs. (4) and (5) are then computed for these images by slicing the 3×3-analysis window pixel by pixel. Finally, the W and Γ values obtained for both image subsets are employed to build the histograms of these parameters. Figure 3 represents the energy histograms for the rainfall echoes in brown and the ground ones in blue. These plots are clearly separated for $W = 0.04$.

In most cases: $W < 0.04$ for ground echoes and $W > 0.04$ for rainfall echoes. Thanks to such a threshold, the ground clutter can therefore be suppressed and rainfall echoes, preserved in the images under study. Similarly, Fig. 4 exhibits the homogeneity histograms for rainfall and ground echoes in brown and blue respectively. We get that: $\Gamma < 0.55$ for ground echoes and $\Gamma > 0.55$ for rainfall echoes. This threshold also enables us to remove the fixed ground clutter and keep almost all the rainfall echoes unchanged. When applying either the energy or homogeneity threshold to the radar images under study, the central pixel analyzed by the 3×3 window will be replaced by a black point if this pixel belongs to a ground echo and remains unchanged if it is assigned to a rainfall echo.

To illustrate the methodology described above, both the filters respectively based on energy and homogeneity thresholds, were applied to the image of Fig. 1. For example, we have shown in Fig. 5 the result of the filtering technique using the energy parameter. This image shows the persistence of a great number of residual small cells. To reduce this ground clutter, the median filter was then used. The images of Fig. 6 arise from the radar echo filtering using energy and homogeneity thresholds respectively and the median filter.

Notice that with both types of filter, only few percent of these echoes are not correctly reproduced owing to the slight overlaps respectively observed in the energy and homogeneity

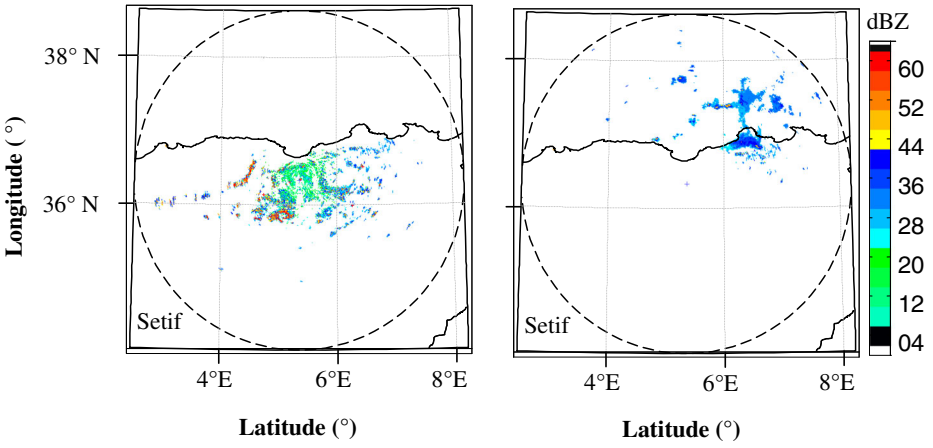

Fig. 2 Images of ground clutter and rainfall for Setif

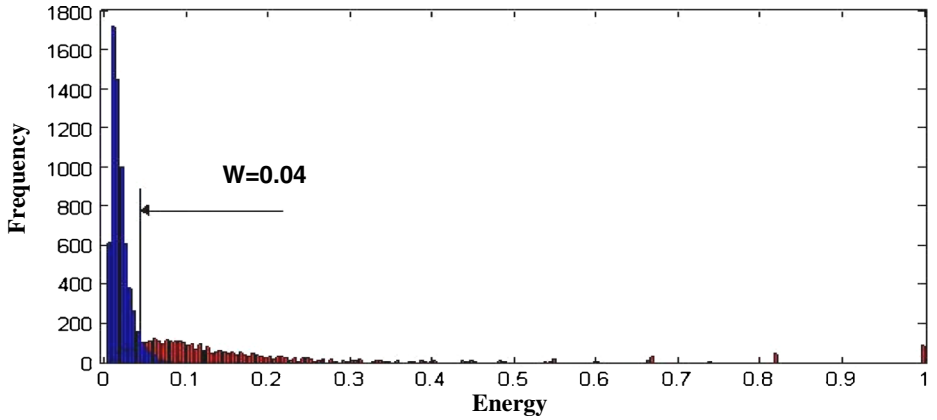

Fig. 3 Histograms of energy for rainfall (*brown*) and ground (*blue*) echoes

histograms. These images show that the ground clutter is removed more efficiency with the local homogeneity parameter. Moreover the application of the median filter has the effect of spreading colors on all these clouds and distorting their real structure.

5 Template Associated with Patter Recognition Technique

5.1 Template Method

The radar data base used was divided into two categories by using image processing software. One gathers the clear sky images contain only ground clutter, and the other consists of images where the rain echoes are accompanied by the ground clutter. The application of the template method for the radar images requires passage through two steps: [16]

- **Construction of the template:** The masking technique used to filter the radar images, is primarily based on the construction of templates that form an image of the mountains

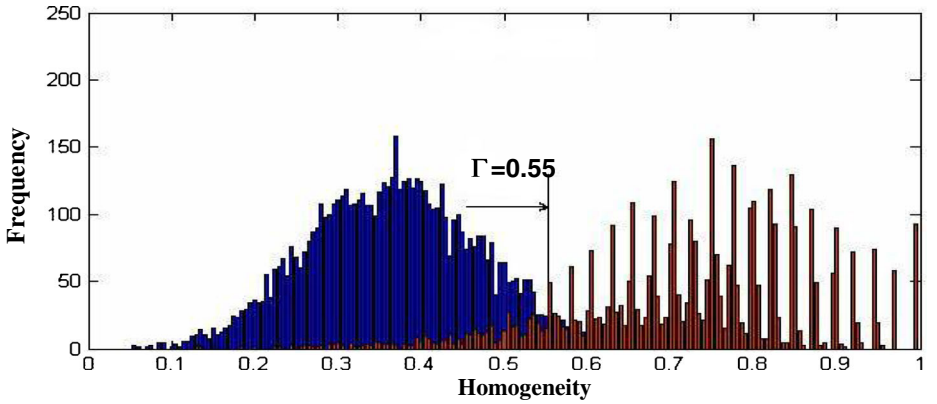

Fig. 4 Homogeneity histograms for rainfall (*brown*) and ground (*blue*) echoes

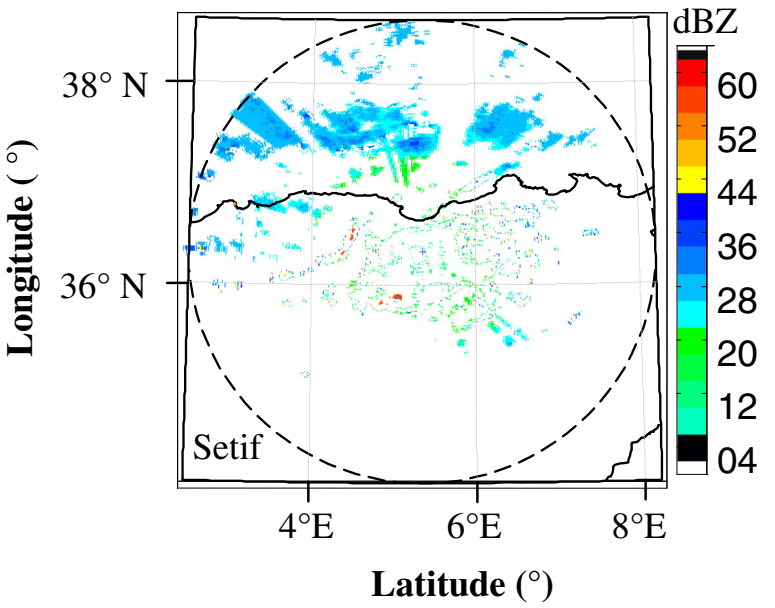

Fig. 5 Radar images of Setif filtered using energy

surrounding the radar. In practice, the template image is composed of pixels whose level of reflectivity is the most frequent. For this purpose, it is built pixel by pixel by averaging a large number of images in clear sky.

- **Filtering images:** To eliminate ground clutter, each raw image is compared, pixel by pixel, for the template image obtained. If the pixels of the two kinds of images have the same level of reflectivity, they are replaced by pixels of zero reflectivity in the raw images. Otherwise, the pixels retain their original reflectivity.

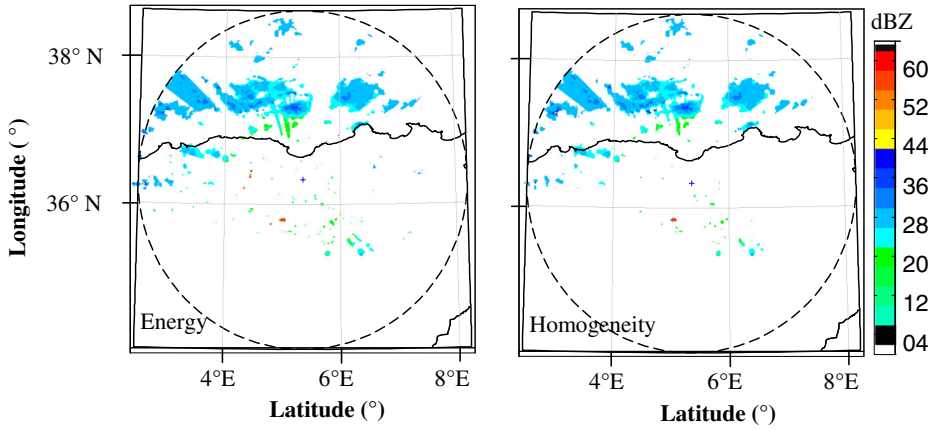

Fig. 6 Radar images filtered by using textural technique

For the construction of the image of template characterizing the region of Setif, 1998 was chosen as a reference because it has nearly 4300 images in clear sky. From these images the template corresponding to this region was constructed and shown in Fig. 7.

The image represented in Fig. 1 was then filtered using the templates method. The result is shown in Fig. 8. It is found that the application of the mask alone cannot filter all the noise cells coming from the ground. Hence, we developed a new method to remove these cells based on pattern recognition.

6 Templates Associated with Pattern Recognition

After removing the ground echoes by the template technique, we improved this technique by combining it with a pattern recognition algorithm that we have developed. This algorithm operates by exploring the image, pixel by pixel, using an analysis window of 3 × 3 pixels. It includes the following steps:

- This window is centered on a pixel surrounded by eight nearest neighbors for the first pixel that does not have a zero reflectivity.
- The cell is detected by counting, for each pixel, the number of neighbors whose have a non-zero reflectivity. If more than seven nearest neighbors have zero reflectivity, the analyzed pixel is replaced by a zero. If at least one of its neighbors has their reflectivity different from zero, the pixel is assigned to the cell studied. Then, it is stored with its coordinates position and reflectivity value.
- The surface of each detected cells is evaluated by counting the pixels that compose it. This area is recorded if it is greater than 20 km^2, as a rain echo. If it is less than 20 km^2, no recording is done because we are in the presence of ground spots.

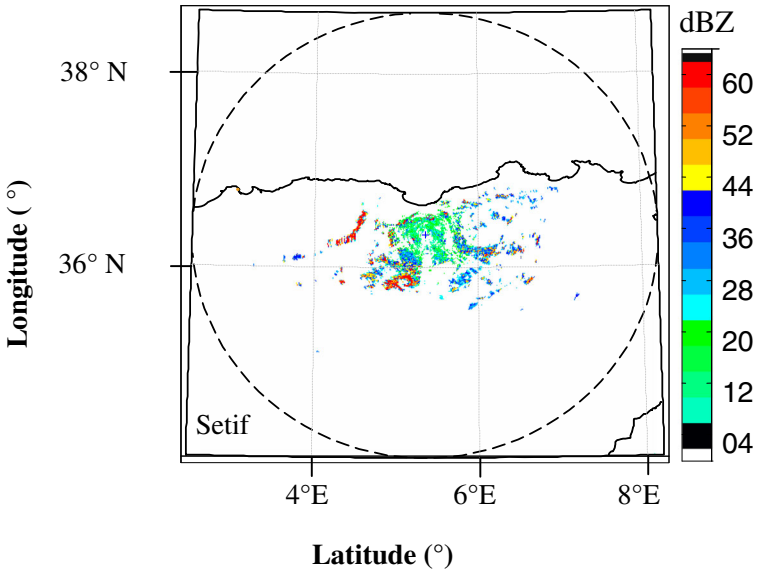

Fig. 7 Template image for Setif region

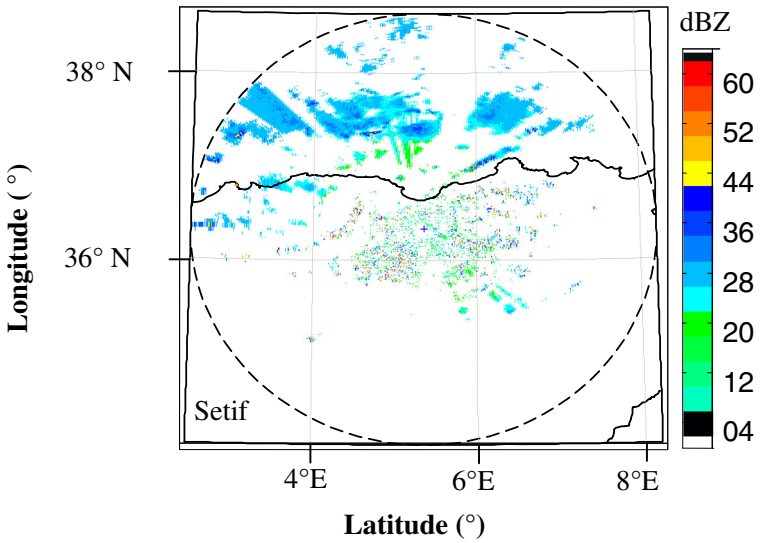

Fig. 8 Result of applying the template technique to the image of Fig. 1

Figure 9 shows the result of filtering the images represented by the Fig. 1 by using the template and pattern recognition. This image shows that the rain cells are properly restored and all the ground spot has been eliminated. Ground clutter could therefore be effectively removed without changing precipitation echoes.

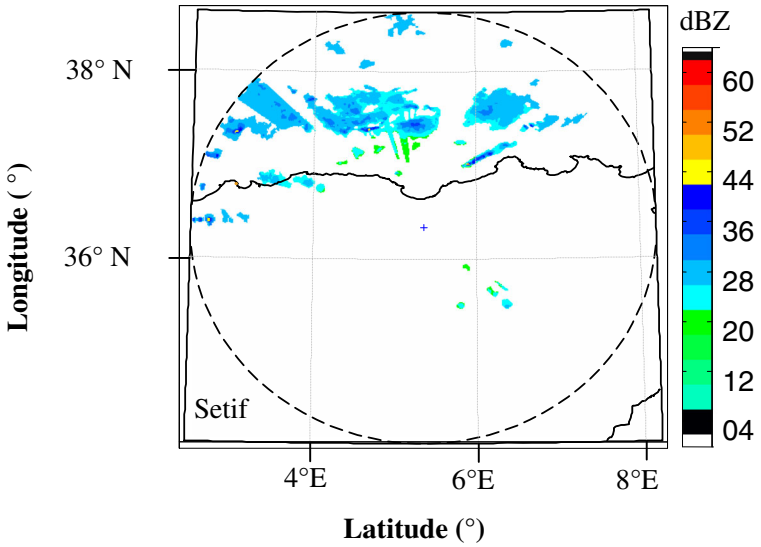

Fig. 9 Result of applying the template associated with pattern recognition to the image of Fig. 1

7 Comparative Study

To test the effectiveness of our method, we evaluated the losses surfaces caused by the filtering techniques developed in this paper for the image of Setif shown in Fig. 1 and two other images recorded in Bordeaux (France) and Dakar (Senegal).

For these types of images taken in three different regions, we calculated the surface S of precipitation echoes obtained by using the various methods described above (SADH with energy parameters and local homogeneity, with and without median filtering, templates and templates with median filter and pattern recognition). Each raw image has previously been used to construct a reference image wherein the surface S_0 of the precipitation echo was totally preserved and the ground clutter has been removed manually using Photoshop software. This gives S_0 = 17461 km^2 for Setif, 30295 km^2 for Bordeaux and 34019 km^2 for Dakar. Then, each filtered surface S resulting from each method has been compared to the reference surface S_0. Finally losses filtering surfaces were evaluated by s = (S - S_0) / S_0. A positive value of the report s indicates an increase in surface caused by deformations due to filtering and a negative value indicates a decrease resulting from alterations by this filtering. The result values are reported in Table 1. This table shows that the filter with the templates associated with median filter gives good results compared to those obtained using the SADH energy or local homogeneity. Note also that the filtering template gives very low surface except that this surface is not precipitation echoes but a ground spot (See Fig. 8). With the method of template associated with pattern recognition losses surfaces are negligible and practically all ground echoes were eliminated. In addition, the application of this method does not change the shape or color of the precipitation echoes.

The template method takes several hours to make the image of clear sky, depending on the size of the clear-sky database and the computer resources, but once the template is implemented, the applying of this algorithm is instantaneous. In the case of the SADH, the calculation time required does not exceed 30 s, depending primarily on the number of nonzero pixels in the image to be filtered. The method of templates associated with pattern recognition takes less than 60 s. This time depends mainly on the size of the cells observed

Table 1 Surface of precipitation echoes after filtering using different methods

Filtering method	Site					
	Setif S_o = 17461 km^2		Bordeaux S_o = 30295 km^2		Dakar S_o = 34019 km^2	
	S (km^2)	s (%)	S (km^2)	s (%)	S (km^2)	s (%)
SADH with W	41741	−15,5	23966	−20,8	31949	−6
SADH with Γ	13963	20	23526	−22,3	31906	−6,2
Templates	20848	19	30516	0,7	34133	0,3
SADH with W + median filter	14390	−15,5	23538	−22,3	32050	−5,7
SADH with Γ + median filter	13635	−22	23135	−23,6	32088	−5,6
Templates + median filter	17672	1.2	30189	−0,3	34189	0,5
Templates associated with pattern recognition	17288	−0,9	30163	−0,4	33699	−0,9

(with, W = energy, Γ local homogeneity, S_0 = raw surface)

in the radar image. However, this method can easily operate in real time because the radar images are taken at a rate of one image in a better time of 5 min.

8 Restoration of Precipitation Echoes by Optimization Algorithm

Figure 10 shows a radar image taken in Bordeaux where rainfall echoes overlap with ground clutter and the resulting image of the application of the method of template associated with pattern recognition. In this figure, we observe an alteration in the form of a hole in white, indicating the absence of echoes in the middle of the image where the ground echoes are located. However, it is possible to regenerate the lost areas, using a regulation technique based on the interpolation from its neighborhoods.

Widely applied in the restoration of works of art, old photographs and old film recordings, the image interpolation is a method used to restore images by masking or eliminating some unwanted elements in images. Most of these are in the form of grains, stains or

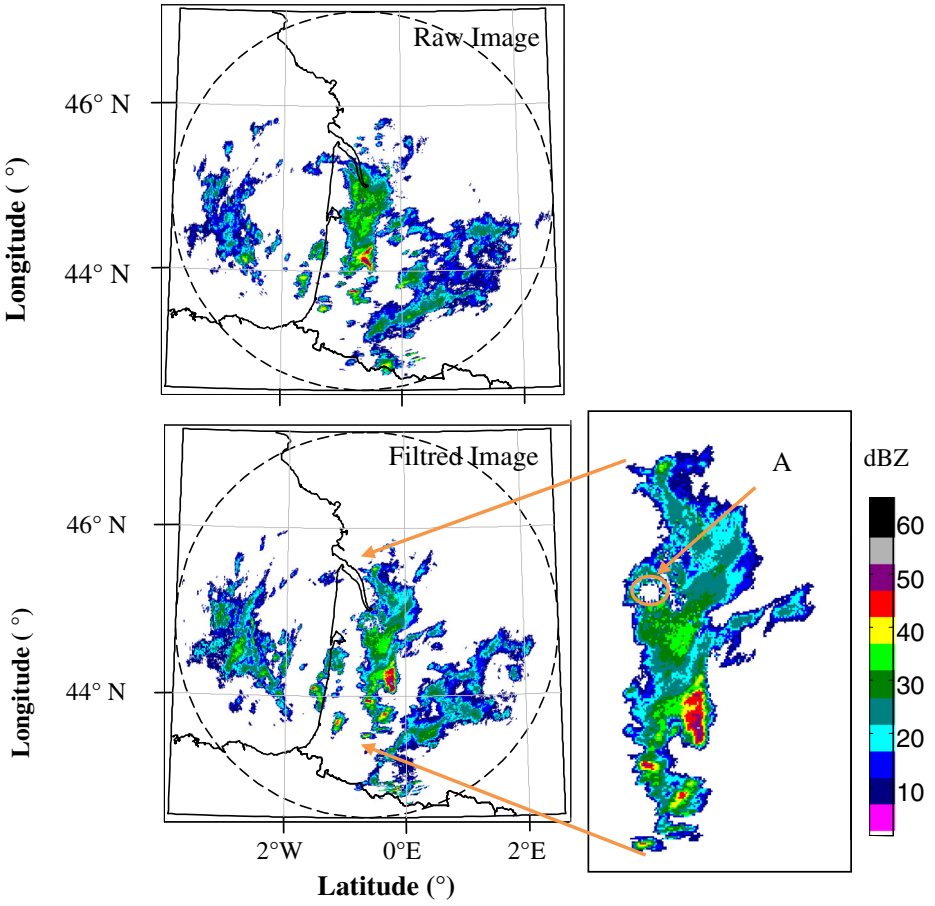

Fig. 10 Appearance of a lacuna (A) in radar image filtered by the templates associated with pattern recognition

footprint thus altering the original images. In image processing, the result of this type of restoration also increases the resolution of the image in color and luminance. Note that the image restoration is widely applied in biology, nuclear physics and telecommunications. Given these advantages, the application of this method to the radar images should help to reconstruct the missing parts of the rainfall echoes.

9 Description

Restoration of radar images is a question not easy to solve because it is regenerate parts of precipitation echoes that were erased when we have filtering the ground clutter. However, it can be resolved on the basis of the restoration of the printed image on a material support and having undergone damage. For this, the most widely used technique is based on optimization [17–19]. Its principle is to reconstruct the image areas that have been affected by restoring their reflectivity by interpolation from neighboring pixels that are still intact. In the problem of radar images retouching, digital image I includes damage or gaps that act as a noise Nb in addition to the pure image restore U. These images are related by a matrix equation which is written:

$$I = U + Nb \tag{6}$$

To determine the nature of the noise Nb, preliminary tests were performed on the radar images. They involve using, alternatively, the Gauss-Laplace distributions, Laplace distribution and the Poisson model for describing the alterations in these images. It is found that the image restoration algorithms converge faster and give better results when the noise is Gaussian. The restoration technique of radar images used is based on optimizing a cost function which represents the image to be reconstructed, with the constraint of the influence of the neighborhood of the intact regions. Under these conditions, we used an improved version of the Bregman algorithm, which is the Split Bregman algorithm because it allows as solving effectively and quickly this kind of optimization [17–19]. To optimize this function, the Split Bregman algorithm operates by solving this equation:

$$\hat{U} = \underset{\mathrm{U,F}}{\operatorname{argmin}} \left\{ \sum_{m,n} \left|\mathrm{f}_{m,n}\right| + \frac{\lambda}{2} \sum_{m,n} \left(\mathrm{I}_{m,n} - \mathrm{u}_{m,n}\right)^2 + \frac{\gamma}{2} \sum_{m,n} \left|\mathrm{f}_{m,n} - \nabla \mathrm{u}_{m,n} - \mathrm{b}_{m,n}\right|^2 \right\} \tag{7}$$

The matrix elements $f_{m,n}$ are deduced from the relation $F = \nabla U$ expressing transitions between intact regions and altered zones, λ and γ are adjustment parameters obtained after several iterations and $b_{m,n}$ parameters form a matrix B deduced by the recurrence relation:

$$B^{k+1} = B^k + \nabla U^{k+1} - F^{k+1} \tag{8}$$

The matrixes B characterize the influence of the intact area to reconstitute pixels, and k is the number of iterations. The parameter γ is the weight of the constraint $F = \nabla U$ while λ acts substantially on the power noise. In practice, the Eqs. (7) and (8) are solved using the Gauss-Seidel which reduces to solving the recurrence equation [19]:

$$U_{m,n}^{k+1} = G_{m,n}^{k} \tag{9}$$

with

$$G^k_{m,n} = \frac{\lambda}{\beta+4\lambda}\left(u^k_{m+1,n}+u^k_{m-1,n}+u^k_{m,n+1}+u^k_{m,n-1}+f^k_{x,m-1,n}-f^k_{x,m,n}\right)+\frac{\lambda}{\beta+4\lambda}$$
$$\left(f^k_{y,m,n-1}-f^k_{y,m,n}-f^k_{x,m-1,n}+f^k_{x,m,n}-f^k_{y,m,n-1}+f^k_{y,m,n}\right)+\frac{\beta}{\beta+4\lambda}I_{m,n} \tag{10}$$

F is the matrix formed from components $f_{m,n}$ and β is a constant of adjustment.In particular, this algorithm is used to calculate the parameters $b_{m,n}$ and $u_{m,n}$ in the direction downward and upward until the Split Bregman algorithm converges reaching a defined tolerance:

$$\mathrm{e} = \frac{\left\|\hat{\mathrm{U}}-\mathrm{U}\right\|}{\|U\|} \tag{11}$$

10 Application to the Radar Images

After several tests, we found that when $\lambda < 100$, the radar image is very smooth and becomes too distorted. But when λ is greater, the noise is significantly reduced and the image is restored with very few alterations. After several iterations, these parameters reach their optimum value: $\lambda = 10^3$ and $\gamma = 30$. In this case, the image is restored practically without any alteration and with minimal iterations. Figure 11 represents the result of the restoration of the Fig. 10 with a tolerance of 10^{-5}. It shows that the pixels of cloud cells deleted when filtering ground echoes were restored with a little different reflectivity from the neighborhood of the intact pixels. The returned part has a reflectivity that varies descending from the center to the edges and the result looks exactly like a cloud echo as it really appears in a radar image. Therefore, this algorithm has allowed a good reconstruction and filling the lacuna by avoiding the distortion of the other regions of the original image.

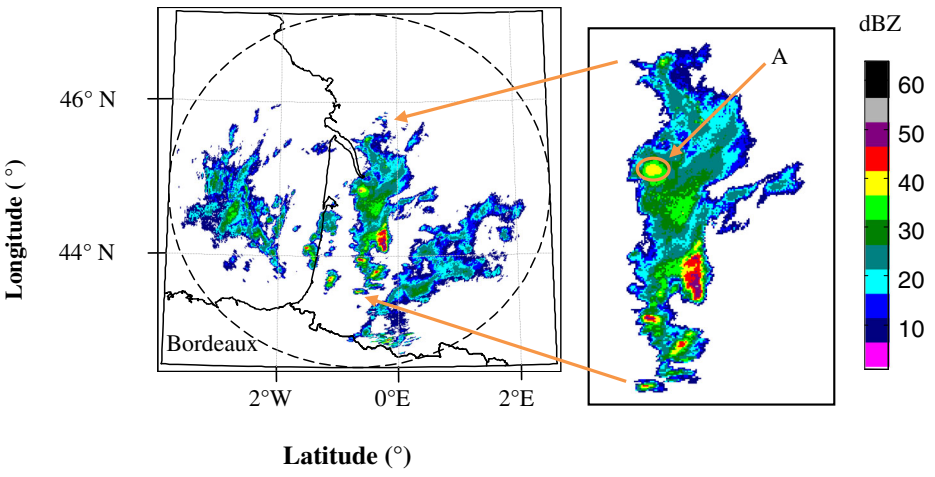

Fig. 11 Restoration of the area affected by filtering with templates associated with pattern recognition. (A: restored area)

11 Conclusion

In this paper we develop different algorithms that allow us to filter ground clutter and preserve the rainfall echoes appearing in the radar images with a sufficiently good accuracy. Considering the textural features of these images, we have found two efficient filters, namely the energy- and homogeneity-based filters, which can clearly distinguish rainfall and fixed ground echoes. Both filters that retain the rainfall echoes by thresholding, yield similar results.

However, it may be interesting to combine both textural features to reduce the histogram overlaps and improve the filtering accuracy. also behaves as an efficient filter for the radar echoes under study. Thanks to the shape detection of these echoes, we have obtained significant improvements that amount to eliminate all the undesirable ground spots in the image. Thus, the template filtering also behaves as an efficient filter for the radar echoes under study. This algorithm reduces the ground clutter and split them into small cells. The application of the templates associated with pattern recognition can effectively remove all residual echoes keeping intact almost all rain clutter. However, we found that this filtering technique strongly affects the rain echoes when they are superimposed on the ground returns. In this case, the interpolation method of split Bregman optimization can reproduce almost all areas of rainy cells. In hydrology, the meteorological radar is suitable for the real time observations of the atmospheric perturbations and the evolution of rainy clouds in a given region. In hydrology, the meteorological radar is suitable for the real time observations of the atmospheric perturbations and the evolution of rainy clouds in a given region. In these conditions, our filtering methods will be very helpful to evaluate the amount of water falling in a given region during the periods of bad weather.

References

1. Chapman, R.N.: Development of sizing nomograms for stand-alone photovoltaic/storage systems. Sol. Eng. **43**, 71–76 (1989)
2. Renaut, D.: Les satellites météorologiques. La Météorologie **45**, 33–37 (2004)
3. Keeler, R.J., Passarelli, R.E.: Signal processing for atmospheric radars. In: Lenschow, D.H. (ed.): Radar Probing and Measurement of the Planetary Boundary Layer, pp. 199–229. American Meteorological Society, Boston (1986)
4. Serafin, R.J.: Meteorological radar. In: Skolnic, M. (ed.): Radar Handbook, 2nd ed, pp. 23.1–23.28. Mc Graw-Hill, New York (1990)
5. Sauvageot, H.: Radar Meteorology. Artech House, Boston (1992)
6. Taylor, J.W.: Receivers. In: Skolnik, M.I. (ed.): Radar Handbook, 2nd ed, pp. 3.1–3.54. McGraw-Hill, New York (1990)
7. Darricau, J.: Physique et théorie du radar, T.2: Principes et performances de base, Sodipe, Paris (1993)
8. Meischner, P.: Weather Radar: Principles and Advanced Applications. Springer, Berlin (2005)
9. Haddad, B., Adane, A., Sauvageot, H., Sadouki, L., Naili, R.: Identification and filtering of rainfall and ground radar echoes using textural features. Int. J. Remote. Sens. **25**(21), 4641–4656 (2004)
10. Haralick, R.M., Shanmugam, K., Dinstein, I.: Textural features for image classification. IEEE Trans. Syst. Man Cybern. **SMC-3**(6), 610–621 (1973)
11. Weszka, J.S., Dyer, C.R., Rosenfeld, A.: Comparative study of texture measures for terrain classification. IEEE Trans. Syst. Man Cybern. **SM-6**, 269–285 (1976)
12. Unser, M.: Sum and difference histograms for texture classification. IEEE Trans. Pattern. Anal. Mach. Intell. **PAMI-8**(1), 118–125 (1986)
13. Chen, D.W., Sengupta, S.K., Welch, R.M.: Cloud field classification based upon high spatial resolution textural features, simplified vector approaches. J. Geoph. Res. **94–D12**, 749–765 (1989)
14. Wang, L., He, D.C.: A new statistical approach for texture analysis. Photogramm. Eng. Remote. Sens. **56**(1), 61–66 (1990)

15. Ameur, Z., Ameur, S., Adane, A., Sauvageot, H., Bara, K.: Cloud classification using the textural features of Meteosat images. Int. J. Remote Sens. **25**(21), 4491–4503 (2004)
16. Raaf, O., Adane, A.: Image-filtering techniques for meteorological radar. In: International Symposium on Industrial Electronics, IEEE ISIE08, Cambridge (2008)
17. Bregman, L.M.: The relaxation method of finding the common points of convex sets and its application to the solution of problems in convex optimization. USSR Comput. Math. Math. Phys. **7**, 200–217 (1967)
18. Rudin, L.I., Osher, S., Fatemi, E.: Nonlinear total variation based noise removal algorithms. Phys. D **60**, 259–268 (1992)
19. Goldstein, T., Osher, S.: The Split Bregman method for l1-regularized problems. SIAM J. Imaging Sci. **2**(2), 323–343 (2009)